



## Performance of the CAPRICE98 balloon-borne gas-RICH detector

D. Bergström<sup>a,\*</sup>, M. Boezio<sup>a,1</sup>, P. Carlson<sup>a</sup>, T. Francke<sup>a</sup>, S. Grinstein<sup>a</sup>,  
N. Weber<sup>a</sup>, M. Suffert<sup>b</sup>, M. Hof<sup>c</sup>, J. Kremer<sup>c</sup>, W. Menn<sup>c</sup>, M. Simon<sup>c</sup>,  
S.A. Stephens<sup>d</sup>, M. Ambriola<sup>e</sup>, R. Bellotti<sup>e</sup>, F. Cafagna<sup>e</sup>, M. Castellano<sup>e</sup>,  
F. Ciaccio<sup>e</sup>, M. Circella<sup>e</sup>, C. De Marzo<sup>e</sup>, N. Finetti<sup>f</sup>, P. Papini<sup>f</sup>, S. Piccardi<sup>f</sup>,  
P. Spillantini<sup>f</sup>, S. Bartalucci<sup>g</sup>, M. Ricci<sup>g</sup>, V. Bidoli<sup>h</sup>, M. Casolino<sup>h</sup>,  
M.P. De Pascale<sup>h</sup>, A. Morselli<sup>h</sup>, P. Picozza<sup>h</sup>, R. Sparvoli<sup>h</sup>, G. Barbiellini<sup>i</sup>,  
P. Schiavon<sup>i</sup>, A. Vacchi<sup>i</sup>, N. Zampa<sup>i</sup>, J.W. Mitchell<sup>j</sup>, J.F. Ormes<sup>j</sup>,  
R.E. Streitmatter<sup>j</sup>, U. Bravar<sup>k</sup>, S.J. Stochaj<sup>k</sup>

<sup>a</sup> Royal Institute of Technology, Stockholm, Sweden

<sup>b</sup> Centre des Recherches Nucléaires, Strasbourg, France

<sup>c</sup> Universität Siegen, Siegen, Germany

<sup>d</sup> Tata Institute of Fundamental Research, Bombay, India

<sup>e</sup> INFN Section and Physics Department, University of Bari, Bari, Italy

<sup>f</sup> INFN Section and Physics Department, University of Firenze, Firenze, Italy

<sup>g</sup> Laboratori Nazionali INFN di Frascati, Frascati, Italy

<sup>h</sup> INFN Section and Physics Department, University of Tor Vergata, Roma, Italy

<sup>i</sup> INFN Section and Physics Department, University of Trieste, Trieste, Italy

<sup>j</sup> NASA/Goddard Space Flight Center, Greenbelt, USA

<sup>k</sup> New Mexico State University, Las Cruces, USA

Received 2 October 2000; accepted 28 October 2000

### Abstract

A RICH counter using a gas radiator of C<sub>4</sub>F<sub>10</sub> and a photosensitive MWPC with pad readout has been developed, tested in particle beam at CERN and used in the CAPRICE98 balloon-borne experiment. The MWPC was operated with a TMAE and ethane mixture at atmospheric pressure and used a cathode pad plane to give an unambiguous image of the Cherenkov light. The induced signals in the pad plane were read out using the AMPLEX chip and CRAMS. The good efficiency of the Cherenkov light collection, the efficient detection of the weak signal from single UV photons together with a low noise level in the electronics of the RICH detector, resulted in a large number of detected photoelectrons per event. For  $\beta \simeq 1$  charge one particles, an average of 12 photoelectrons per event were detected. The reconstructed Cherenkov angle of 50 mrad for a  $\beta \simeq 1$  particle had a resolution of 1.2 mrad (rms). The RICH was flown with the CAPRICE98 magnetic spectrometer and was the first RICH counter ever used in a balloon-borne experiment capable of identifying charge one particles at energies above 5 GeV. The RICH provided an identification of

\*Corresponding author. Tel.: +46-8-16-10-93; fax: +46-8-15-86-74.

E-mail address: david@particle.kth.se (D. Bergström).

<sup>1</sup> Also at Sezione INFN di Trieste, Trieste, Italy.

cosmic ray antiprotons up to the highest energies ever studied (about 50 GeV of total energy). The spectrometer was flown on 28–29 May 1998 from Fort Sumner, New Mexico, USA. © 2001 Elsevier Science B.V. All rights reserved.

*PACS:* 29.40.Ka; 98.40.De; 98.70.Sa

*Keywords:* Cherenkov detector; Balloon instrumentation; Cosmic rays

---

## 1. Introduction

A gas Ring Imaging Cherenkov counter (RICH) has been developed, tested in particle beams at CERN and flown in the CAPRICE98 balloon-borne experiment [1,2]. The detector was built to identify cosmic rays [3–6] in the rigidity range 2–330 GV.

The CAPRICE98 spectrometer science objectives were to measure the antimatter component in the cosmic rays in the energy range 2–50 GeV and to study the cosmic ray composition in the atmosphere in the energy region between a few hundred MeV and 330 GeV. The main goal of the gas RICH detector was to identify antiprotons in a large background of electrons, atmospheric and locally produced negative pions and muons. Since the first observation by Golden et al. [7] there has been several experiments measuring the energy spectrum of antiprotons in the cosmic rays. The energy spectrum has recently been determined with good accuracy below 4 GeV kinetic energy ([8] and references therein). The observed spectrum indicates that the cosmic ray antiprotons are mostly of secondary origin, produced by the collision of cosmic ray nuclei with interstellar gas. Above 4 GeV only two measurements exist [7,9], both with low statistics, and which give very different flux values.

The detection of antiprotons at high energies is an experimental challenge due to the difficulty in detecting and identifying the antiprotons against a vast background. Sophisticated particle identification detectors are therefore needed to identify the rare antiprotons. The information from the gas RICH combined with the information from the other detectors in the CAPRICE98 magnetic spectrometer provided excellent particle identification. The RICH detector described in this paper is

capable of mass resolving protons/antiprotons between 18 and 50 GeV [10]. Below 18 GeV it acts as an efficient threshold Cherenkov detector for proton/antiproton identification.

The spectrometer was one of the most complex instrument ever flown in a balloon-borne experiment for cosmic ray studies. The apparatus included a tracking system with three drift chambers [11], a time-of-flight system, a gas RICH counter, a silicon-tungsten imaging calorimeter [12,13] for particle identification and a 4T superconducting magnet [14]. It was launched with a balloon from Fort Sumner, New Mexico, on 28th May 1998 and floated at an atmospheric depth of about 5.5 g/cm<sup>2</sup> (corresponding to an altitude of about 36 km) for a period of 21 h, at a mean vertical cutoff rigidity of about 4.5 GV. Information about more than 5 million cosmic ray particles was collected during the flight.

## 2. The gas RICH detector

The RICH detector [3–6], shown in Fig. 1, consisted of a photosensitive multiwire proportional chamber (MWPC) and a 1 m tall radiator box, filled with high purity C<sub>4</sub>F<sub>10</sub> gas at an average pressure of 911 mbar. As illustrated in Fig. 1, charged cosmic ray particles ionized the gas in the MWPC before entering into the gas radiator, where Cherenkov light was emitted along the particle track. The Cherenkov light was reflected and focused by a spherical mirror back onto the photosensitive MWPC where the position of the Cherenkov light was accurately determined. The RICH was sensitive to light in the wavelength region 165–220 nm limited by the transmission of the quartz window (> 165 nm) and the quantum

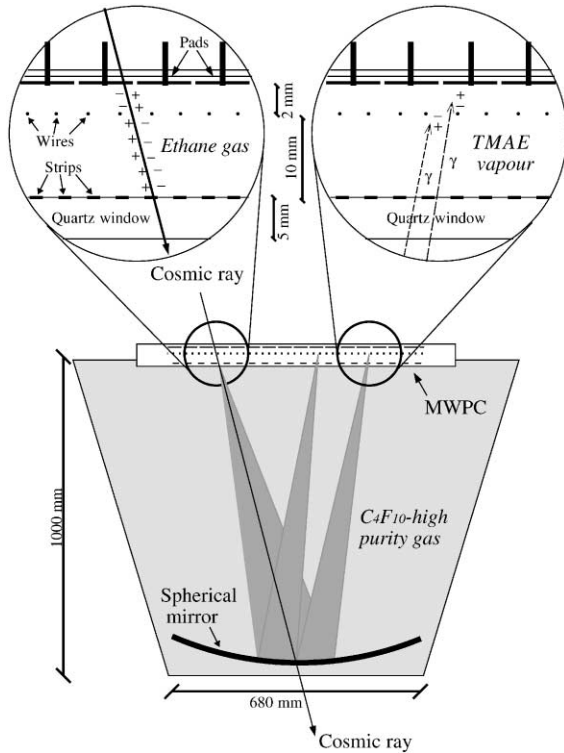


Fig. 1. Schematic view of the CAPRICE98 RICH detector. The left upper expanded view illustrates how the gas in the MWPC is ionized by the cosmic ray particle. The position of the pads, wires and strips are indicated. The “-” and “+” in the figure are referred, respectively, to electrons and ions liberated in the ethane gas. In the lower part the Cherenkov light emitted in the  $C_4F_{10}$  gas close to the particle track is indicated by the shaded area. A spherical mirror reflects the light back up onto the MWPC. In the right upper expanded view, two Cherenkov photons ( $\gamma$ ) enter the MWPC through the quartz window where they each liberate one photoelectrons from the TMAE vapour.

efficiency of the TMAE<sup>2</sup> ( $<220$  nm). The sensitive area of the detector was  $480 \times 480$  mm<sup>2</sup> defined by the size of the quartz window.

### 2.1. The MWPC

The MWPC consisted of a frame with anode wires between an upper cathode pad plane and a lower cathode of conductive strips on a quartz window. The 128 gold-plated tungsten anode wires

were 15  $\mu$ m in diameter, 4 mm apart and 520 mm long. The cathode pad plane was a sandwich of two 0.5 mm thick Vetronite boards glued on the two sides of a 6 mm thick plate of Rohacell. Both Vetronite boards were plated with copper and gold. The lower board contained 4096 pads. Each pad ( $8 \times 8$  mm<sup>2</sup>) was connected to a pin glued to the board and fed through the pad plane to the backside where it was used as a connector to the front-end electronics. The MWPC was operated with pure ethane saturated with tetrakis-(dimethyl-amino)-ethylene (TMAE), at moderate gain ( $4.4 \times 10^5$ ) in order to minimize photon feedback. A gas system, described in Section 2.3, was used to flush the MWPC with a low constant flow of TMAE saturated ethane gas.

To achieve the high detection efficiency of  $>12$  photoelectrons per event as an average for  $\beta \approx 1$  particles [4], the TMAE had to be heated to 35°C, giving a conversion probability of  $\approx 80\%$  in the 12 mm thick MWPC.

All parts of the gas volumes in the RICH detector that would be in thermal contact with the TMAE had to be heated at all times to prevent the gas from condensating on the inner surfaces of the detector. This required a regulated heating system, which was required work at all times and during all possible operating conditions. The apparatus had to run with all systems active for several weeks continuously, during the integration and preflight testing at ground. The heating systems also had to take care of the temperature control during the flight when the temperature outside the payload could vary between  $-30^\circ\text{C}$  and  $+40^\circ\text{C}$ . The conditions for the instruments inside the gondola, which can be seen in Fig. 2, were however not that extreme, since it was thermally insulated from the outside. The MWPC requires a stable temperature environment to be able to operate reliably. If the temperature of the MWPC was lower than the TMAE saturated ethane gas, then the TMAE would condensate. Discharges in the high voltage induced by the condensated TMAE could destroy the detector.

The 16 channel, low noise, VLSI chip AMPLEX [15] was used for the read out of the anode wires and the cathode pads. Each channel included a charge sensitive pre-amplifier, a shaping amplifier

<sup>2</sup>Tetrakis-dimethyl-amino-ethylene.

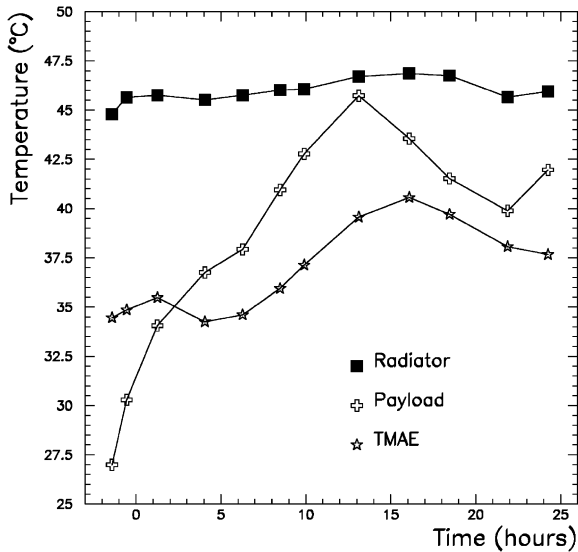


Fig. 2. Temperature variations at float inside the gondola during the CAPRICE98 flight. The graph shows the temperature at different positions inside the gondola. The filled squares are the temperatures in the radiator of the RICH detector. The open crosses are the temperatures inside the payload. The stars are the temperatures of the TMAE liquid. The time is from the time of the launch.

and a track and hold system where the charge was stored before being read out. The AMPLEX chips, 32 for the cathode pads (512 channels) and 8 for the anode wires (128 channels), were daisy-chained and readout in series (multiplexed) and fed to the VME based digital readout electronics, CRAMS<sup>3</sup> (CAEN V550). A CRAMS module has two independent analog to digital conversion blocks, which each can be programmed to read out between 32 and 2016 channels in steps of 32 channels. Therefore, four CRAMS (8 blocks) with 512 channels in each of the two blocks, were used for the cathode pads and one CRAMS (one block) with 128 channels was used for the anode wires. In the CRAMS, each signal was digitized by a 10-bit flash ADC, pedestal subtracted and stored in a memory if the remaining signal exceeded a preset threshold value (usually five times the rms noise). The readout time was 2  $\mu$ s per channel giving a total readout time of approximately 1 ms. The

<sup>3</sup>CAEN Readout for Analog Multiplexed Signals.

trigger rate during the flight was 65 Hz. A typical signal from a single photoelectron was 70 fC (spread out over an average of 3.5 pads) and the equivalent noise of the electronics was 7 fC (rms).

Fig. 3 shows some details of the readout electronics and control system. The trigger logic generated all the control signals (hold, start read and reset) and distributed them to the AMPLEX and VME read out. The external trigger was given by the time-of-flight system. The multiplexed signals from the front-end electronics were sent to the CRAMS where a VME CPU module (SYS68K/IBC-20 FORCE) managed the data handling and storage. After pedestal subtraction of the signal in the CRAMS the data was read by the VME CPU module and made accessible for storage on discs and transmission to ground by the central computer via a VME/Q-bus interface module. The memories in the CRAMS, where the signals were initially stored, could be considered as an extension of the VME CPU memory.

A pedestal and threshold calculation was performed at every start-up of the RICH detector. A computer-induced trigger was fed to the detector and the average noise level for each individual channel was determined. The noise measured was then later subtracted from the signal read out for each event before the data were saved on disks or transmitted via radio link to ground. Important effects that could require a recalculation were large temperature and pressure changes, electronic noise from other instruments, radio noise picked up by the wires in the MWPC, voltage fluctuations in the power feeding the detector, etc. The pedestal and threshold calculation could be performed at any moment when it was found to be necessary for a stable performance of the detector.

In Fig. 4 the output of two CRAMS channels are shown as function of the induced charge in the AMPLEX. The channel to channel gain variations are less than 10%. Above 400 fC the AMPLEX becomes saturated, corresponding to the signal from six photoelectrons in a single channel.

The 5 mm thick quartz window ( $480 \times 480$  mm<sup>2</sup>) was made of Suprasil 3, and had cathode strips evaporated onto it acting as the lower cathode. The strips were 150  $\mu$ m wide, 3 mm apart giving a

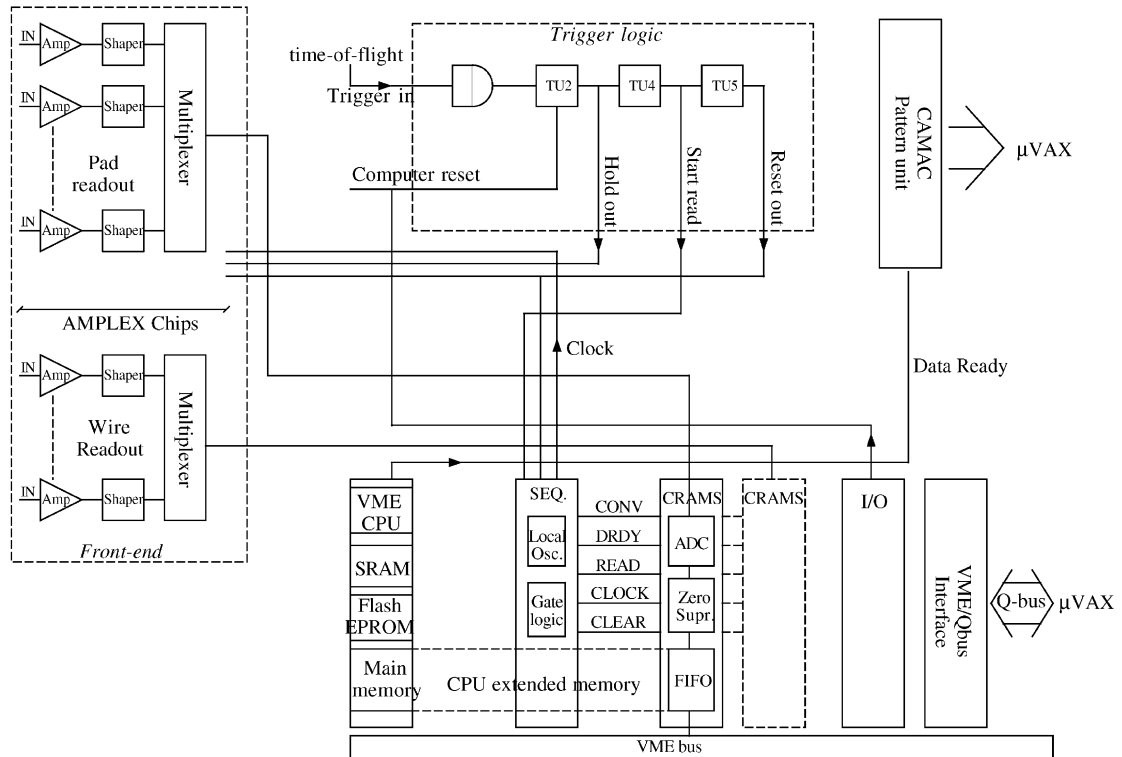


Fig. 3. Schematics of the read out electronics. The trigger logic in the centre takes care of generating all the control signals (hold, start read and reset) and distribute them to the AMPLEX and VME read out. The multiplexed signals from the front-end electronics (AMPLEX) were sent to the CRAMS where the VME CPU module took care of the data handling and storage. The communication between the VME CPU and the trigger logic goes through a VME I/O module. After pedestal subtraction of the signal in the CRAMS, the VME CPU reads out the data. The data is then accessible for the central  $\mu$ VAX via a VME/Q-bus interface for storage on data disks and transmission to ground.

total transmission of 95%, which was independent of the particles angle of incidence since the strips were only 100 nm thick (10 nm nickel + 80 nm copper + 10 nm nickel). The quartz window was glued into a frame of Invar which had the same thermal expansion coefficient as quartz and the frame could move freely with respect to the main frame holding the chamber, in order not to strain the quartz window by thermal expansions. The quartz window was transparent for wavelengths longer than 165 nm [16].

## 2.2. The radiator

The radiator was build to have the largest possible acceptance and to withstand a vertical

impact shock of about 10 g. Because of weight constraints, aluminium was used as material for all the enclosure and for the support structure. The radiator box had to be absolutely airtight not to affect the purity of the  $C_4F_{10}$  gas. The internal volume of the radiator box was 800 l with two inlets and two outlets. One inlet was only used during the first phase when the dry nitrogen was added to the system and was then disconnected and closed during the second ( $C_4F_{10}$  filling) and third (cleaning) phases. One inlet and one outlet were used for circulating the gas through the radiator. The gas flow was regulated so that the pressure in the radiator would at all times be a few mbar above the payload pressure. This was intended to prevent large pressure drops in the

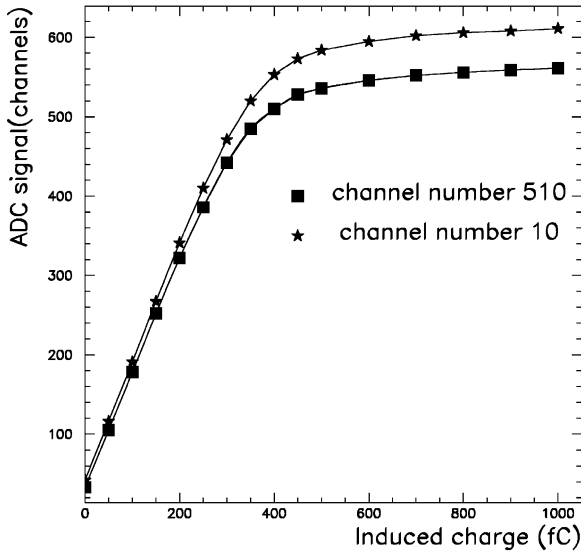


Fig. 4. The output signal of the CRAMS as a function of the charge injected into the AMPLEX. Note that above 400 fC the AMPLEX becomes saturated. The amplitude of the output signal and saturation limit for these two channels are typical for the response of all pad channels.

radiator, which could cause its thin aluminium box to implode, and also to prevent the payload gas (mostly nitrogen) to leak into the radiator. Due to the risk of failure of the radiator, there was an overpressure relief system connected to the second outlet with two oil filled bubblers with an intermediate balloon filled with cleaned gas. Thus, this dual system protected the gas system from contamination due to small changes of pressure differences between the radiator and the payload, while at the same time protecting the radiator box from exploding because of a sudden large input of gas into the radiator.

2.3. The gas system

The overall purpose of this gas system was to separate and clean the C<sub>4</sub>F<sub>10</sub> gas used in the CAPRICE98 RICH radiator from all other gases and especially from water and oxygen, since oxygen will absorb Cherenkov photons and

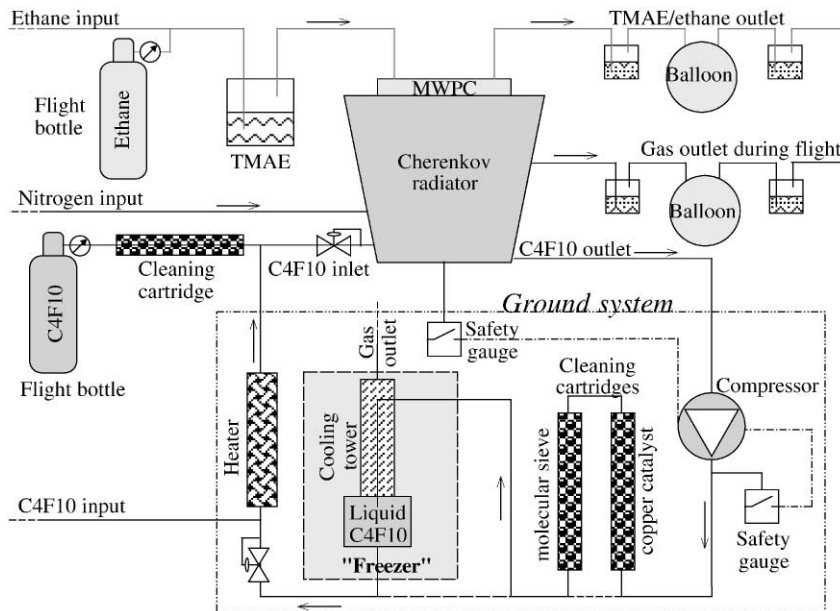


Fig. 5. The complete gas system for TMAE/ethane and C<sub>4</sub>F<sub>10</sub> used by the gas RICH detector. In the upper part of the figure can be seen the MWPC with the connected input and outlet for ethane through bubblers. The lower part of the figure shows the C<sub>4</sub>F<sub>10</sub> gas system for filling and cleaning of the Cherenkov radiator. This system contains of, besides the radiator volume, a compressor, two cleaning cartridges and a freezer. Two gas bottles that provided the RICH detector with the ethane and C<sub>4</sub>F<sub>10</sub> used during the flight, were located inside the payload.

thereby reduce the efficiency of the detector. The cleaning was performed in three steps. First the radiator volume was flushed with several cubic meter of nitrogen. This had the purpose of drying out the whole system and get rid of as much air and moisture as possible. The following step was a process in which the  $C_4F_{10}$  (99.96% guaranteed by the manufacturer) was let in to the system and at the same time the nitrogen was separated and expelled from the system using the combination of a freezer and a compressor. Finally, the  $C_4F_{10}$  gas was purified by filtering it through two cleaning cartridges. The  $C_4F_{10}$  gas system was designed to keep the impurities of oxygen below 0.12% (upper limit), which was sufficient for having a more than 50% transmission of Cherenkov light.

We show in Fig. 5 the complete gas cleaning system and the gas system for the ethane/TMAE mixture of the MWPC. The system could be divided into two major parts, one internal part that was situated inside the CAPRICE98 payload and one external part only used during ground operations with most of the components mounted in a rack that had to be positioned close to the payload. All the gas tubes connecting these two parts of the system had to be fed through the

payload shell with vacuum tight connectors without restraining the circulation of the gas.

The gas cleaning system had two different modes of operation (shown in Fig. 6): One for filling and cleaning of the gas during the preflight ground operations, and a simplified version for the flight. The full ground support system included a compressor, a cleaning section and a freezer. The compressor circulated the gas through the cleaning system and the radiator volume. The large pressure also increased the vapour pressure and gave a more efficient cleaning procedure. A cartridge filled with a copper catalyst was used to split water molecules and then a cartridge with a molecular sieve removed oxygen. Any hydrogen and nitrogen left in the system was expelled in the freezer. The simplified flight version only consisted of a gas bottle with 10 l of prepurified  $C_4F_{10}$  liquid sufficient for about 70 h of operation and a cartridge with the catalysator and molecular sieve combined. Since this bottle was only intended to be used during the flight, the cartridge was connected to the system just before the regulated input of the radiator and the bottles regulator was set to open only when the pressure was lower than the output pressure from the freezer.

The compressor, which was connected to the first outlet of the radiator, had the function of circulating the gas through the system. The gas was extracted from the radiator and the pressure was increased, so that the  $C_4F_{10}$  gas would easily liquify in the freezer kept at  $-40^\circ\text{C}$ . In case of a sudden decrease of the pressure in the radiator, a pressure sensor would automatically shut down the compressor. The  $C_4F_{10}$  that went back into the radiator was taken from this liquid, which guaranteed that no other gases, like nitrogen and oxygen which would still be in gas form at this pressure and temperature, could reenter the radiator. These unwanted gases were instead expelled out of the system through an outlet valve. The remaining contamination of oxygen in the radiator, after usage of the cleaning system, was measured during the test at CERN to be as low as 230 ppm [4]. This was then a stable situation during all the experiment and was well below the limit that was needed to get the required efficiency for the Cherenkov light collection.

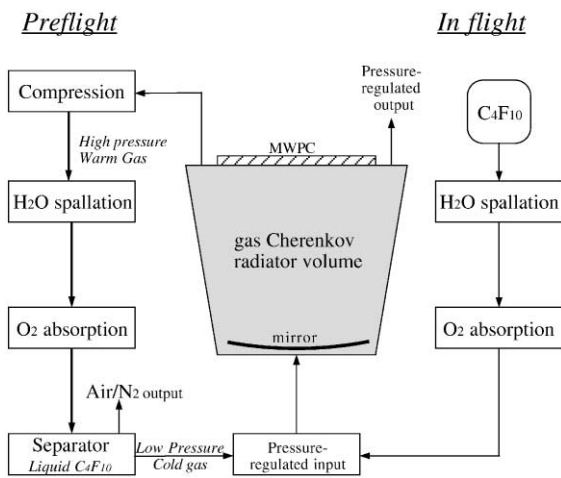


Fig. 6. The operation principle of the ground and flight  $C_4F_{10}$  gas systems. The left side of this system was used during ground operations. The right side shows the flight system, which went into operation only during the flight.

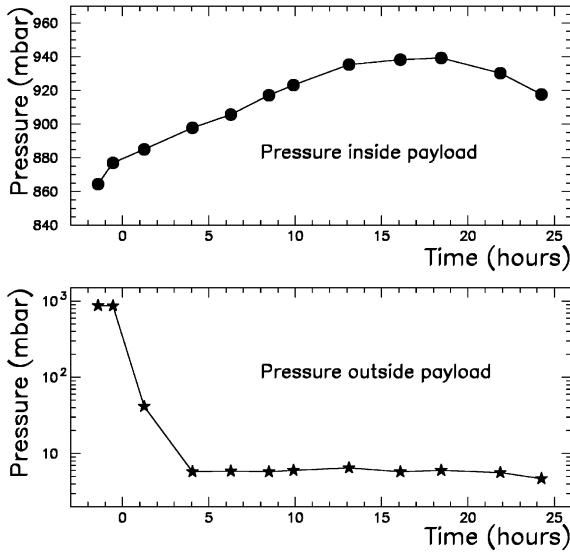


Fig. 7. Pressure variations at float inside the gondola during the CAPRICE98 flight. The filled bullets are the pressures inside the payload and the stars are the pressure outside the payload. The times on both graphs are from the time of the launch.

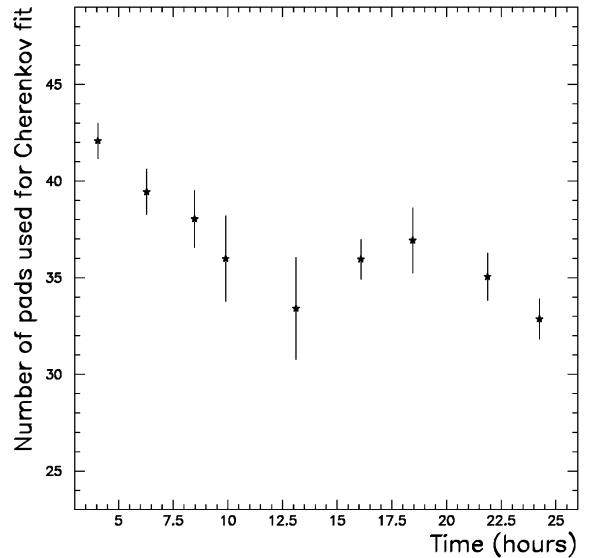


Fig. 8. The average number of pad hits that was used for the Cherenkov angle calculation, which is proportional to the number of photoelectrons. The time scale starts from the launch of the payload.

### 3. Results from flight data

Fig. 7 shows the payload pressure, which averaged at 911 mbar, and Fig. 2 the mean temperature, with an average of about 45.9°C in the radiator volume, during the CAPRICE98 flight. This resulted in a refractive index of about 1.0014, corresponding to a threshold Lorentz factor of 18.9. The refractive index was estimated using ultrarelativistic particles (electrons) and it was shown [4] to follow precisely the change in the gondola pressure during the whole duration of the CAPRICE98 flight.

Fig. 8 shows the number of pads used for the Cherenkov angle calculation,  $n_{\text{eff}}$ , for  $\beta \simeq 1$  particles during the flight.  $n_{\text{eff}}$  (Eq. (2)) is directly proportional to the number of photoelectrons. The slow decrease with time that can be seen in the figure was due to increasing contamination in the radiator. This decrease was partly compensated by the increasing pressure during the flight.

Fig. 9 shows a selection of events of different species, as detected by the RICH detector. The top

left view shows an example of the Cherenkov ring in the pad plane from a proton, with a rigidity of 38.8 GV measured by the tracking system. Each square corresponds to one pad hit. The filled squares were selected as originating from Cherenkov light and open squares were either due to ionization or electronic noise. The big circle was obtained from the radius derived from the fitted Cherenkov angle  $\theta_c$  (Eq. (1)). The “+” is the expected centre of that circle, extrapolated from the reconstructed track given by the tracking system. A small circle and an “X” are located at the position where the particle crossed the multi-wire proportional chamber according to the RICH detector and the tracking system, respectively. The arrow shows the direction of the incident particle. The lower left figure shows an electron with a measured rigidity of 3.7 GV. The electron is fully relativistic and therefore the Cherenkov angle is at its maximum of about 51 mrad, corresponding to a ring diameter of about 11 cm. The upper right figure shows a helium nuclei with a measured rigidity of 95.6 GV. Important to notice is the

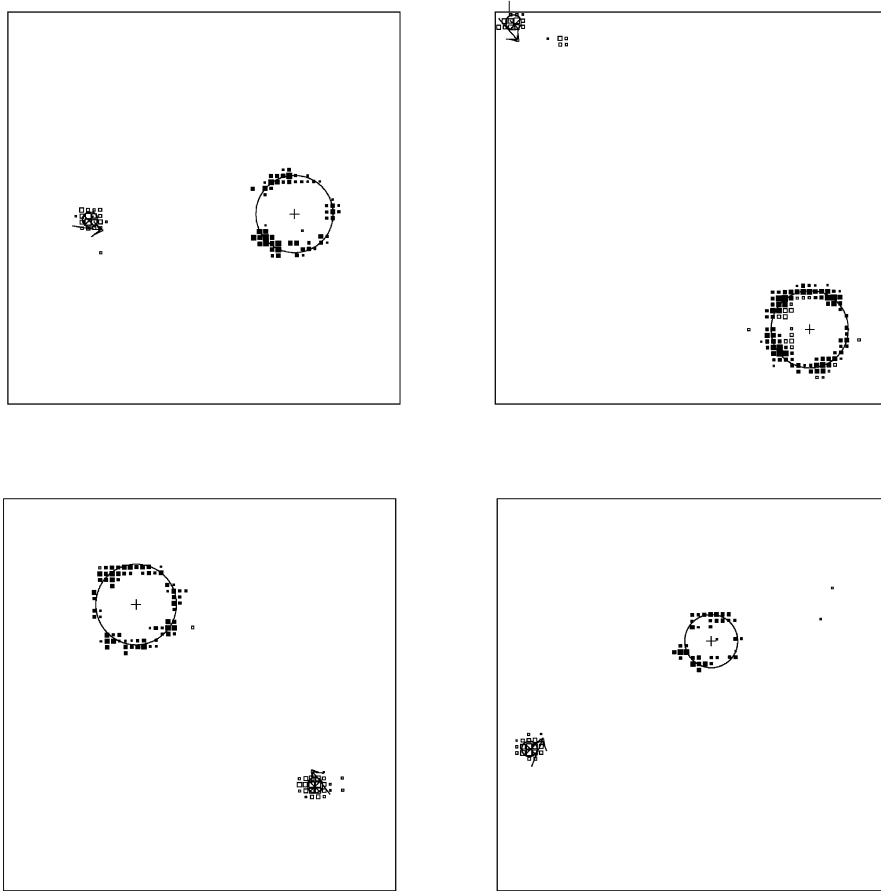


Fig. 9. A selection of different hit patterns in the RICH pad plane from different particle species: The upper left figure shows the ionization and ring of Cherenkov light of a selected proton with a measured rigidity of 38.8 GV. The lower left figure is an electron at its maximum Cherenkov angle with a measured rigidity of 3.7 GV. The upper right figure shows a helium nucleus with a measured rigidity of 95.6 GV. The lower right figure shows an antiproton at a measured rigidity of 22.7 GV. The big circle in each figure was obtained from the radius derived from the fitted Cherenkov angle. The “+” is the center of the circle predicted by the tracking system. A small circle and an “X” are located at the position where the particle hits the multiwire proportional chamber according to the RICH detector and the tracking system, respectively. The size of the pad plane (indicated by the square border) is  $51 \times 51 \text{ cm}^2$ . An arrow shows the direction of the incident particle.

much larger amount of Cherenkov light produced by this particle. The lower right figure shows an antiproton at a measured rigidity of 22.7 GV. The threshold rigidity to produce Cherenkov light for (anti)protons in the gas RICH detector was about 18 GV. Already at rigidities of 25 GV, an average of six photoelectrons were detected.

A charged particle that crossed the multiwire proportional chamber induced a signal in several pads, of which at least one was a saturated signal.

The particle impact position in the RICH can therefore be determined with a centre of gravity calculation using the pads closest to the largest signal, which was the one most likely to be at the position of the track. A saturated pad has a signal that is typically 10 times larger than a signal coming from a Cherenkov photon. Since the size of the MWPC was not covering the whole acceptance of the tracking system, only 33% of the events, which had the centre of the Cherenkov

ring in the MWPC, would have an ionization signal from the particle track going through the MWPC. Note also (in Fig. 9), the clean appearance of the ring of Cherenkov light and the very low number of noise induced signals. This was important for particles with velocities below the threshold of Cherenkov light production, when the RICH was used as a threshold device. For identification of antiprotons between 2(3) GeV/ $c$ , which was the threshold for muons(pions), and 18 GeV/ $c$ , which was the threshold for antiprotons, this could be used since the high number of photoelectrons detected assured that muons and pions would produce a distinct Cherenkov light signal. An important feature, when using the RICH detector as a threshold device, was that it was not only using a “light/no-light” condition, but the tracking system gave information about where in the pad plane the Cherenkov light should have been detected, thereby greatly enhancing the detector immunity to noise. Less noisy pads, on the average, than one out of 4096 channels per event was detected, allowing a stringent selection of antiprotons where no signals should appear in the predicted area, still maintaining a high identification efficiency. All 4096 channels were working during the entire flight.

Since the signal induced by one photoelectron was picked up by 3–5 pads, one approach would be to do a centre of gravity calculation over these pads, weighing them by their signal value and from this deduce the Cherenkov angle for each individual Cherenkov photon. However, in most cases the probability that one pad could get part of its signals from at least two different photoelectrons was high because of the large number of photoelectrons. This made it difficult to estimate how much of the induced charge in a pad came from each photoelectron. Therefore, each pad was treated separately in the Cherenkov angle calculation. The signal amplitude, with its information of amount of induced charge, was not used for the same reason.

The Cherenkov angle was calculated for each pad that was not included in the  $9 \times 7$  pad ionization area closest to the track, using an iterative geometrical method. This method used the “Fermats principle” that light uses the path

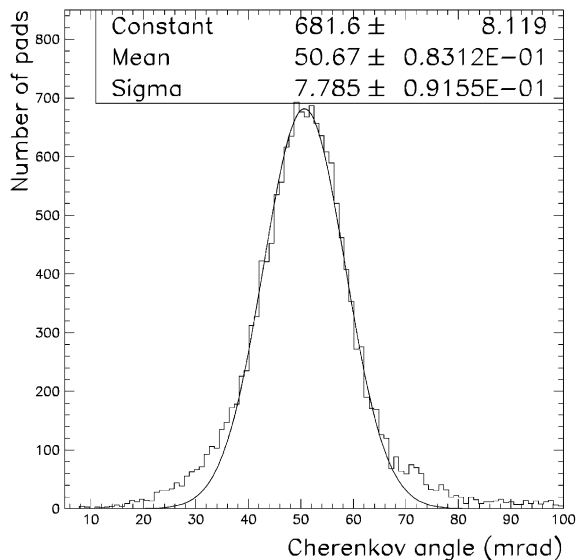


Fig. 10. The Cherenkov angle distribution for single pads for  $\beta \simeq 1$  electrons and muons selected from flight data. The Gaussian fit gives a resolution ( $\sigma$ ) of 7.8 mrad for a single pad.

that gives the shortest possible time for travelling between two points. For this calculation we used: the position of the pad where the signal was induced, the position of the mirror and the direction of the particle (given by the tracking system) at the point where the Cherenkov light was emitted. Since the point of emission for the Cherenkov light was not determined, it was assumed that the light was emitted half-way between the MWPC and the mirror.

The Cherenkov angle  $\theta_c$  for the whole event was calculated using a so called “Gaussian potential method” [17]. This is an iterative method that assigns a Gaussian weight;

$$\omega_i = e^{-(\theta_i - \theta_c)^2 / 2\sigma_i^2} \quad (1)$$

where  $\theta_i$  and  $\theta_c$  are the Cherenkov angle of each pad and for the whole event, to the Cherenkov angle calculated for each pad, depending on how much it differs from the fitted Cherenkov angle. Fig. 10 shows the reconstructed Cherenkov angle distribution for a large number of single pads. The data used for this distribution are from  $\beta \simeq 1$  electrons and muons selected from flight data. A

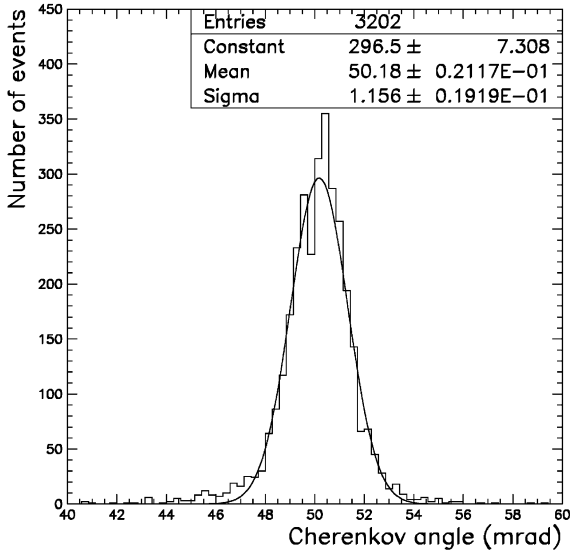


Fig. 11. The Cherenkov angle distribution for selected muons with rigidity greater than 12 GeV/c from ground data. A Gaussian curve is fitted to the distribution.

Gaussian fit has been performed to the region 36–64 mrad. This distribution gives a single pad resolution of 7.8 mrad. The tails of the distribution, which are not included in the fit, are due to the fact that the signal from each photoelectron spreads out over several pads. It has been shown in a previous work on the CAPRICE94 experiment that the Gaussian potential method gives the best result on the Cherenkov angle determination [18]. The multiwire proportional chamber and the calculation routines used for the CAPRICE98 experiment were the same as were used for the CAPRICE94 experiment. The Gaussian potential method had the benefit that pads with Cherenkov angles far from the mean value, with signals due to e.g. electronic noise, were suppressed.

The measured Cherenkov angle for a large sample of data taken at ground a few days before the CAPRICE98 flight are shown in Fig. 11. This sample of particles with a measured rigidity greater than 12 GV contains mostly muons. A Gaussian curve is fitted to the distribution and shows a resolution of about 1.3 mrad for  $\beta \simeq 1$  particles with a Cherenkov angle of 50 mrad. The

refractive index, which depends on the pressure, was measured to be 1.0012, which corresponds to a maximum Cherenkov angle of 50.0 mrad.

It is difficult to estimate the number of photoelectrons from the data, because of the overlapping of the signal from different photoelectrons. The signal induced in a pad could be from more than one photoelectron. A large number of photoelectrons, typically more than 20, would give so many overlaps that it would create a “full” ring. For most particles detected by the RICH detector this is not the case though.

We estimated the number of photoelectrons on an event-by-event basis. A number of electrons from a large sample of flight data were selected and the number of clusters, which should correspond to one photoelectron, was counted. The result was a mean value of  $12 \pm 2$  photoelectrons per event. This result was cross checked by studying the dependence of the efficient number of pad hits used for the Cherenkov angle calculation:

$$n_{\text{eff}} = \frac{(\sum_i^{n_{\text{pads}}} \omega_i)^2}{\sum_i^{n_{\text{pads}}} \omega_i^2} \quad (2)$$

where  $\omega_i$  (Eq. (1)) is the weight of the Cherenkov angle of that pad. For the calculation a fixed value for  $\sigma_i$  was used, which was the average measured Cherenkov angle resolution for a single pad (7.8 mrad).  $n_{\text{eff}}$  is closely related to the number of pad hits due to Cherenkov light and therefore to the number of photoelectrons ( $N_{\text{ph}}$ ), which is related to the Cherenkov angle ( $\theta_c$ ) through [19]:

$$N_{\text{ph}} \propto N_0 L Z^2 \sin^2 \theta_c \quad (3)$$

where  $N_0$  is the detector response parameter (given in  $\text{cm}^{-1}$ ),  $L$  is the distance the particles travel in the Cherenkov light producing gas (in cm) and  $Z$  is the electric charge. A Gaussian fit was made to  $n_{\text{eff}}$  for a large number of  $\beta \simeq 1$  particles. It was then assumed that the full-width at half-maximum of this distribution divided by  $n_{\text{eff}}$  was proportional to  $1/\sqrt{N_{\text{ph}}}$ , where  $N_{\text{ph}}$  is the number of detected photoelectrons. This result in 15 detected photoelectrons per event. This also gives a response parameter,  $N_0 = 57 \text{ cm}^{-1}$  for the average distance ( $L = 98.5 \text{ cm}$ ) that the particles travel in the radiator of the RICH detector. For this study

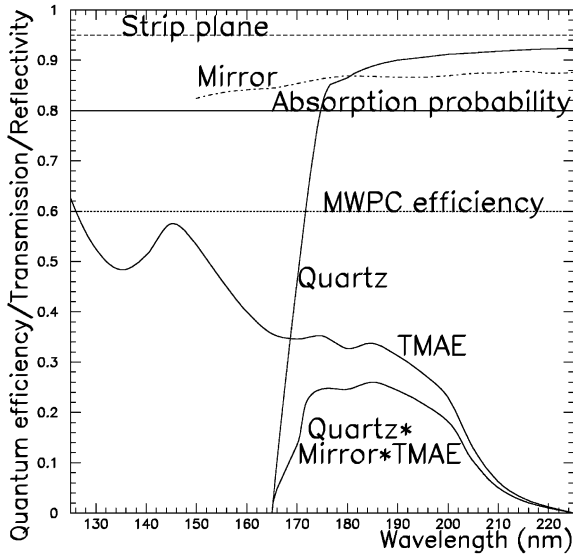


Fig. 12. As a function of wavelength are given: the quantum efficiency of TMAE, the transmission of the 5 mm thick quartz window and the average reflectivity of the spherical mirror. A curve corresponding to the product of the TMAE quantum efficiency, the mirror reflectivity and the quartz window transmission is included. As can be seen from this product, the sensitive region of the RICH detector was 165–225 nm.

negative muons from data at ground were used, since they provide a clean sample of  $\beta \simeq 1$  particles.

An estimation of the number of detected photoelectrons also was made by taking into account the measured reflectivity of the mirror (on average 87%), the quantum efficiency for TMAE, the quartz window transmission (85–90%), the absorption probability (estimated to 80% in the 12 mm of ethane/TMAE gas at 35°C), the strip plane transmission (95%), the transmission of ultraviolet light in  $C_4F_{10}$  (100%) [20] and the efficiency to detect a photoelectron with the MWPC after the pedestal subtraction (60%). Integrating all of the above in the wavelength region 165–225 nm (see Fig. 12) the result was that on the average 14 photoelectrons should be observed for ( $\beta \simeq 1$ ) particles. There was only one unknown factor left, the absorption of light in the remaining contamination of oxygen and water in the radiator. The transmission of light through the radiator depends strongly on the amount of

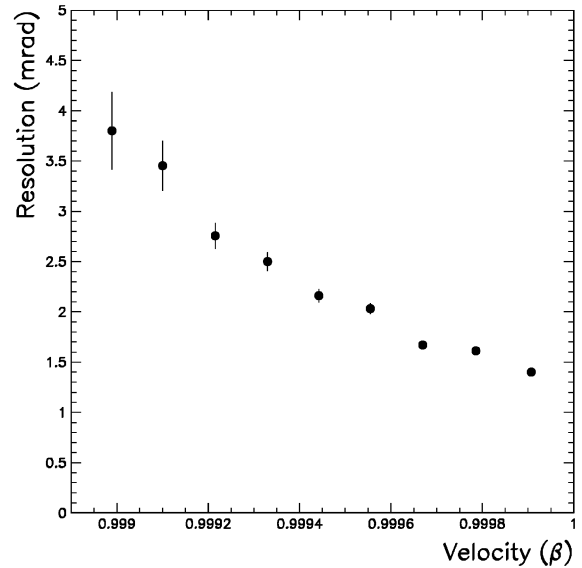


Fig. 13. The measured Cherenkov angle resolution as a function of velocity ( $\beta$ ) of the cosmic ray particle. The resulting resolution for  $\beta \simeq 1$  particles was about 1.2 mrad.

residual oxygen and water contamination in the gas. By comparing the predicted and measured number of photoelectrons we have estimated the transmission to be greater than 85% in the average of 1.5 m that the Cherenkov photons had to travel in the radiator gas before reaching the MWPC.

The Cherenkov angle resolution was determined using a large sample of events. In Fig. 13 it can be seen that the resolution as a function of velocity ( $\beta$ ) varies from 4 mrad close to the threshold of  $\beta = 0.9988$  to about 1.2 mrad for fully relativistic particles. From the average number of photoelectrons ( $N_\gamma = 12$ ), the measured Cherenkov angle resolution ( $\sigma_{\text{tot}} = 1.2$  mrad for  $\beta \simeq 1$ ) and the relation  $\sigma_{\text{tot}} = \sigma_{\text{single}}/\sqrt{N_\gamma}$  then gives a single photoelectron resolution of 4.5 mrad. This is in agreement with the angle resolution for each pad (7.8 mrad) and that each photoelectron on average gives a signal in 3–5 pads.

Besides particle identification on an event-by-event basis, the RICH efficiently rejected multi-particle events. The amplitude of the signal in the pads was used to decide if there were multiple particles passing through the detector. The condition used was that there should not be two

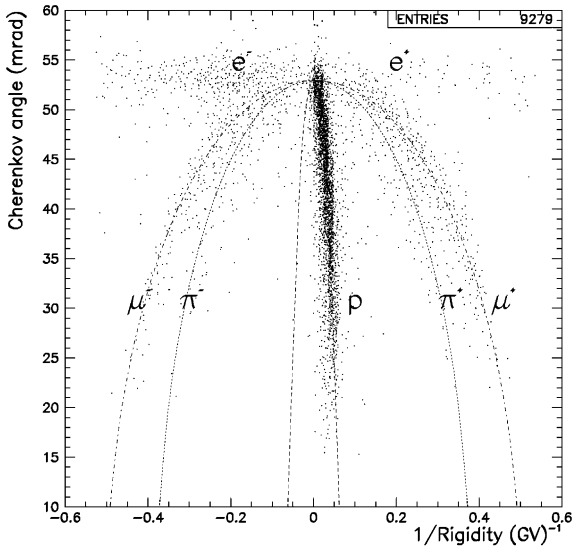


Fig. 14. The reconstructed Cherenkov angle as a function of deflection. The dashed line indicates the expected Cherenkov angle for muons, antiprotons and protons. These are selected charge one events passing the criteria track reconstruction and reconstruction of the Cherenkov angle. The negative section of the rigidity axis is for negatively charged particles.

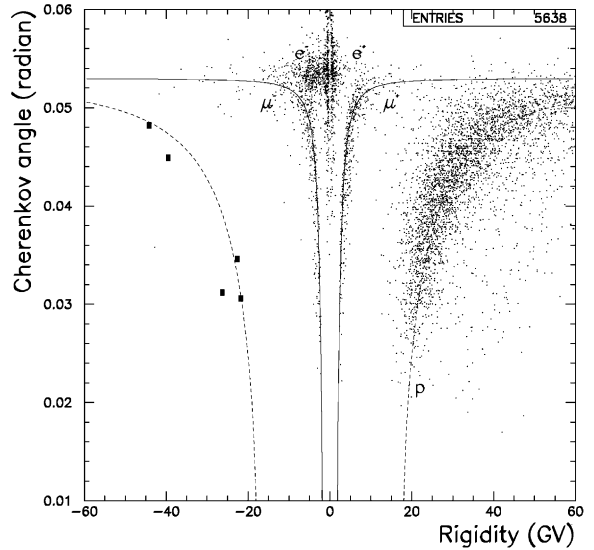


Fig. 15. Shows the Cherenkov angle as a function of rigidity for 5638 charge one particles measured by the CAPRICE98 experiment. To the right is a dense band of protons starting at approximately 18 GV and extending to higher energies and increasing Cherenkov angles. The main bulk of electrons and positrons are located at low energies (below 10 GeV) and at maximum Cherenkov angle. On the negative side, the location of five antiprotons between 20 and 50 GV are indicated by black squares.

saturated pads more than 2 cm apart, because only the ionization by a charged particle could give a saturated signal. Albedo particles with a velocity high enough to produce Cherenkov light in the radiator were rejected by the RICH because the light from such a particle was detected in the wrong part of the MWPC.

Fig. 14 shows the reconstructed Cherenkov angle as a function of deflection up to  $0.6 (\text{GV})^{-1}$  for positive and negative charge one particles collected during flight. These events were chosen for passing good track reconstruction conditions and the conditions on the reconstruction of the Cherenkov angle. The lines in the figure are the expected Cherenkov angles for protons, pions and muons. A dense band of about 6500 protons is extending from the Cherenkov light threshold at approximately  $0.0056 (\text{GV})^{-1}$  to the very highest rigidities (small deflections) and increasing Cherenkov angles. The main bulk of electrons and positrons are located at maximum Cherenkov angle. The RICH detector plays a

crucial role in the CAPRICE98 experiment by the rejection of background muons and pions events. It is important to notice that, muons and pions can be separated in the rigidity region 2–6 GV. This is the first time that this has been done in a balloon-borne experiment. This also shows that the RICH detector allows to very precisely identify muons in the atmosphere, which are important cross-check for the simulations carried out to calculate the atmospheric neutrino fluxes [21].

Fig. 15 shows the measured Cherenkov angle for 5638 particles in the rigidity region up to 60 GV measured by the CAPRICE98 experiment. These were selected charged one events from flight data passing the criteria of the track and the Cherenkov angle reconstruction.

The momentum resolution of the RICH is comparable to the momentum resolution of the CAPRICE98 tracking system up to 50 GeV/c, and in the region 19–28 GeV/c even superior. The maximum detectable rigidity for the tracking

system was 330 GV. The RICH could therefore be used to crosscheck, up to about 70 GeV/ $c$ , the momentum measurement done by the tracking system and to determine the efficiency of the tracking system. This gives the CAPRICE98 experiment a very precise understanding of the systematic uncertainties related to the tracking system.

#### 4. Conclusion

A gas RICH detector using C<sub>4</sub>F<sub>10</sub> gas as radiator has been developed and tested in particle beams at CERN. It has been an important part of a balloon-borne magnet spectrometer experiment, CAPRICE98, which measured the antimatter component in the cosmic rays and the cosmic ray composition in the atmosphere. It allowed cosmic ray antiprotons with energies above 18 GeV to be mass resolved for the first time.

Because of the large number of detected photoelectrons and the low noise level in the MWPC, a good velocity ( $\beta$ ) identification was possible by the induced signal on the pad plane originating from the Cherenkov light. By combining the RICH counter information on Cherenkov angle with the rigidity information in the magnetic spectrometer and the identification capability of the imaging calorimeter of the CAPRICE98 experiment, particles could be fully identified over large energy ranges.

In conclusion, the gas RICH detector performed well during the CAPRICE98 flight and has shown to fulfil all the design requirements.

#### Acknowledgements

We would like to thank the Gas Work Group (EST/SM/SF) and the Thin Films & Section (EP/TA1/TF) at CERN for helping us to construct the gas cleaning system and the mirror. We would like to thank the LEPSI and CRN-Strasbourg who helped us building and construct-

ing the detector and the readout electronics. Finally, we would also like to thank the Particle Astrophysics Lab at New Mexico State University for all their help during the integration and testing of our instrument before the CAPRICE98 flight, as well as the National Scientific Balloon Facility (NSBF) crew for executing the flight.

This work was supported by the Swedish National Space Board and the Knut and Alice Wallenberg Foundation.

#### References

- [1] M. Ambriola et al., Nucl. Phys. (Proc. Suppl.) B 78 (1999) 32.
- [2] M.L. Ambriola et al., Proceedings of the 26th International Cosmic Ray Conference, Salt Lake City, Vol. 5, 1999, p. 17.
- [3] G. Barbiellini et al., Proceedings of the 25th International Cosmic Ray Conference, Durban, Vol. 5, 1997, p. 1.
- [4] D. Bergström, Performance of the CAPRICE98 gas RICH detector, Lic. Thesis, Royal Inst. of Tech., Stockholm, Sweden, 1999 (can be found at [http://msia02.msi.se/group\\_docs/astro/research/references.html](http://msia02.msi.se/group_docs/astro/research/references.html)).
- [5] D. Bergström et al., Proceedings of the 26th International Cosmic Ray Conference, Salt Lake City, Vol. 5, 1999, p. 80.
- [6] T. Francke et al., Nucl. Instr. and Meth. Phys. (Proc. Suppl.) A 433 (1999) 87.
- [7] R.L. Golden et al., Phys. Rev. Lett. 43 (1979) 1264; Astrophys. Lett. 24 (1984) 75.
- [8] S. Orito et al., Phys. Rev. Lett. 84 (2000) 1078.
- [9] G. Basini et al., Proceedings of the 26th International Cosmic Ray Conference, Salt Lake City, Vol. 3, 1999, p. 77.
- [10] D. Bergström et al., Astrophys. J. 534 (2000) L177.
- [11] M. Hof et al., Nucl. Instr. and Meth. A 345 (1994) 561.
- [12] M. Bocciolini et al., Nucl. Instr. and Meth. A 370 (1996) 403.
- [13] M. Ricci et al., Proceedings of the 26th International Cosmic Ray Conference, Salt Lake City, Vol. 5, 1999, p. 49.
- [14] R.L. Golden et al., Nucl. Instr. and Meth. 148 (1978) 179.
- [15] E. de Beuville et al., Nucl. Instr. and Meth. A 288 (1990) 157.
- [16] WISAG, Suprasil II, Products Handbook, 1988.
- [17] T. Ullrich et al., Nucl. Instr. and Meth. A 371 (1996) 243.
- [18] P. Carlson et al., Nucl. Instr. and Meth. A 349 (1994) 577.
- [19] T. Ypsilantis, J. Seguinot, Nucl. Instr. and Meth. A 343 (1994) 30.
- [20] G. Lenzen et al., Nucl. Instr. and Meth. A 343 (1994) 268.
- [21] M. Boezio et al., Phys. Rev. Lett. 82 (1999) 4757.